# Spastin is a dual-function enzyme that severs microtubules and promotes their regrowth to increase the number and mass of microtubules

Yin-Wei Kuo (郭殷瑋)[a,b], Olivier Trottier[a,c], Mohammed Mahamdeh[a,d], and Jonathon Howard[a,1]

[a]Department of Molecular Biophysics and Biochemistry, Yale University, New Haven, CT 06511; [b]Department of Chemistry, Yale University, New Haven, CT 06511; [c]Department of Physics, Yale University, New Haven, CT 06511; and [d]Massachusetts General Hospital, Harvard Medical School, Boston, MA 02129

Edited by Eva Nogales, University of California, Berkeley, CA, and approved February 1, 2019 (received for review November 1, 2018)

**The remodeling of the microtubule cytoskeleton underlies dynamic cellular processes, such as mitosis, ciliogenesis, and neuronal morphogenesis. An important class of microtubule remodelers comprises the severases—spastin, katanin, and fidgetin—which cut microtubules into shorter fragments. While severing activity might be expected to break down the microtubule cytoskeleton, inhibiting these enzymes in vivo actually decreases, rather increases, the number of microtubules, suggesting that severases have a nucleation-like activity. To resolve this paradox, we reconstituted *Drosophila* spastin in a dynamic microtubule assay and discovered that it is a dual-function enzyme. In addition to its ATP-dependent severing activity, spastin is an ATP-independent regulator of microtubule dynamics that slows shrinkage and increases rescue. We observed that spastin accumulates at shrinking ends; this increase in spastin concentration may underlie the increase in rescue frequency and the slowdown in shortening. The changes in microtubule dynamics promote microtubule regrowth so that severed microtubule fragments grow, leading to an increase in the number and mass of microtubules. A mathematical model shows that spastin's effect on microtubule dynamics is essential for this nucleation-like activity: spastin switches microtubules into a state where the net flux of tubulin onto each polymer is positive, leading to the observed exponential increase in microtubule mass. This increase in the microtubule mass accounts for spastin's in vivo phenotypes.**

spastin | severing enzyme | severase | microtubule nucleation | microtubule dynamics

Microtubules are dynamic cytoskeletal polymers that play central roles in cell division, intracellular transport, cell migration, signaling, and cellular morphogenesis (1–3). The morphology and dynamics of microtubule networks are important for their versatile cellular functions. Microtubules have a distinct feature, termed dynamic instability, in which they switch between growing and shrinking phases (4). It is thought that, during growth, GTP-tubulin molecules are incorporated at the microtubule tips and form a stabilizing cap. The loss of this cap due to GTP hydrolysis or subsequent phosphate release leads to catastrophe: the transition from the growing phase to the shrinking phase (5, 6). The reestablishment of the cap leads to rescue: the transition from the shrinking phase to the growing phase. A central question is how various microtubule-associated proteins modulate the assembly and disassembly of existing microtubules as well as generate new microtubules (nucleation) as they remodel cellular microtubule arrays to meet the ever-changing needs of living organisms.

The microtubule-severing enzymes katanin, spastin, and fidgetin are AAA proteins that sever microtubules in an ATP-dependent manner. The founding member of this superfamily, katanin, was first purified from sea urchin egg cytoplasm, where it was thought to break down the interphase microtubules before formation of the mitotic spindle during cell division (7). Severases differ from other microtubule depolymerases, which function primarily at the microtubule ends (8), by binding to and generating internal breaks in the microtubule lattice (9). Previous work has found that severing enzymes are crucial for various biological processes, including mitotic and meiotic spindle formation (10, 11), cilia resorption (12), organization of plant cortical microtubule arrays (13, 14), axonal outgrowth, and neuronal morphogenesis (15–18). Despite their biological importance, how severing enzymes regulate the organization and dynamics of microtubule network remains unknown.

Microtubule severing was first thought of as a destructive process promoting the disassembly of microtubules into the free tubulin pool (7, 18). However, subsequent in vivo studies reported the paradoxical observation that disruption of severing enzyme activity actually leads to a decrease of microtubule density in different systems. The first example of such a phenotype was that a loss-of-function spastin mutant reduced presynaptic microtubules in *Drosophila* neuromuscular junctions (16) [but see Trotta et al. (18)]. Related phenotypes have been observed in several other systems: RNAi knockdown and mutations of the *Caenorhabditis elegans* katanin homolog *mei-1* decreased the number of microtubules in the oocyte meiotic spindle (19), knockdown of spastin caused loss and defects of axonal microtubules in the spinal cords of zebrafish embryos

## Significance

**Microtubule-severing enzymes are ATPases that utilize ATP hydrolysis to fragment microtubules. These enzymes play central roles in various cellular functions, including cell growth and division and neural development. In vivo studies have shown that severing enzymes can lead to an increase in microtubule mass, but how severing activity and microtubule dynamics collectively expand the microtubule network remains unclear. Here, we demonstrate that the severing enzyme spastin is a dual-microtubule regulator: in addition to its severing activity, it promotes microtubule regrowth through an ATP-independent mechanism. Using a mathematical model, we show that the modulation of dynamics is essential for increasing microtubule mass and identify quantitative criteria that must be satisfied if severing is to expand the microtubule network.**

Author contributions: Y.-W.K. and J.H. designed research; Y.-W.K. and O.T. performed research; Y.-W.K. and M.M. analyzed data; Y.-W.K., O.T., and J.H. participated in the mathematical modeling and theory; M.M. provided technical expertise; and Y.-W.K. and J.H. wrote the paper.

The authors declare no conflict of interest.

This article is a PNAS Direct Submission.



[1]To whom correspondence should be addressed. Email: jonathon.howard@yale.edu.

This article contains supporting information online at www.pnas.org/lookup/suppl/doi:10.1073/pnas.1818824116/-/DCSupplemental.

Published online March 5, 2019.

(20), and mutation of the katanin ortholog in *Drosophila* diminished the EB1-labeled microtubule comets in dendrites and affected branching morphology (21). These findings all suggest that severing proteins have a nucleation-like activity by which they increase the number of microtubules and thereby increase the microtubule mass.

A common explanation for this phenomenon is that microtubules cut by severases act as nucleation templates to support new microtubule growth (19, 22, 23). This hypothesis, however, conflicts with the GTP cap model of dynamic instability. According to this model, a break generated by severing enzymes on microtubules should create two GDP-tubulin–exposed ends: the ends are expected to be unstable, and the two newly generated microtubule fragments should shrink and disappear unless stabilized at their ends, perhaps by other microtubule-associated proteins (23, 24). Thus, severing should decrease the number and total mass of microtubules, which contradicts the in vivo findings.

To address this paradox, a recent paper (25) reported that spastin and katanin have an ATP-dependent lattice exchange activity by which GTP-tubulin in solution is transferred into severase-damaged microtubule walls. This activity is proposed to create "GTP islands" in the lattice (26, 27), which both promote microtubule rescue before severing and stabilize the microtubule plus end after severing. The combination of rescue and new end stabilization was proposed to lead to microtubule amplification, although no evidence was presented and no argument was made as to whether these two properties were necessary or sufficient to increase microtubule mass. Additionally, previous studies have shown that free tubulin in solution strongly inhibits the severing activity by reducing the binding of katanin to the microtubule lattice (28, 29), suggesting that lattice damage and GTP-tubulin incorporation may also be inhibited by free tubulin.

To determine how severases increase microtubule mass, we reconstituted spastin in vitro in the presence of tubulin. We found that, in addition to its ATP-dependent severing activity that creates more shorter microtubules, spastin has an ATP-independent promotion of microtubule regrowth (slowing of shrinkage and increasing rescues), which switches microtubules into a state where the net flux of tubulin onto each polymer is positive so that the newly severed microtubules can regrow. A mathematical model of microtubule dynamic instability that includes severing predicts that the severing and regrowth activities lead to an exponential increase in microtubule mass, which we confirmed experimentally. Because spastin-catalyzed lattice exchange requires ATP hydrolysis, yet its rescue promotion effect does not, the lattice exchange/GTP islands mechanism is not necessary for increasing microtubule number and mass. Our work thus demonstrates that *Drosophila* spastin is a dual-function enzyme combining an ATP-independent modulation of dynamic instability with the ATP-dependent severing activity to increase microtubule number and mass.

## Results

To elucidate possible mechanisms of microtubule regulation by severing enzymes inside cells, we asked if the severing protein spastin has a direct effect on microtubule dynamics. *Drosophila* spastin was expressed and purified (*SI Appendix*, Fig. S1). We first confirmed using total internal reflection fluorescence (TIRF) microscopy that, in the absence of free tubulin, spastin is capable of severing microtubules stabilized by guanosine-5′-[(α,β)-methyleno]triphosphate (GMP-CPP) or taxol at low nanomolar concentration (*SI Appendix*, Fig. S2).

We next studied the effects of spastin on dynamic microtubules in the presence of free tubulin but without ATP so as to avoid the confounding effects of severing. Using interference reflection microscopy (IRM) (Fig. 1*A*) (30), we visualized the growth and shrinkage of unlabeled microtubules in the presence of 8 μM tubulin and GTP; an example is shown in Fig. 1 *B* and *C*. We found that addition of 50 nM spastin, close to the cellular concentration (46.5 nM in HeLa cells and ∼50–100 nM in the neuronal tissues of developing rats) (31, 32), did not change the growth rate (Fig. 1*D*) but strongly decreased the shrinkage rate (Fig. 1*E*). Spastin decreased the catastrophe frequency by approximately one-half (Fig. 1*F*), while it increased the rescue frequency more than 10-fold (Fig. 1*G*). Similar effects were observed without ATP or with adenylyl-imidodiphosphate (AMP-PNP) (Fig. 1 *D*–*G*). No microtubule severing was observed in either case, suggesting that ATP hydrolysis is required for severing as previously argued (7, 33). Thus, in addition to being a severase, *Drosophila* spastin is a regulator of microtubule dynamics that reduces the shrinkage rate and promotes rescue (summarized in Table 1).

We next asked if spastin can sever dynamic microtubules and whether severing dynamic microtubules can increase microtubule density in vitro. We fixed fluorescently labeled GMP-CPP microtubule seeds to the chamber surface and grew dynamic microtubules with unlabeled tubulin. A reaction mix containing spastin, tubulin, and both ATP and GTP was then perfused in. Within 2 min, cut microtubules were observed (Fig. 2*A*, 2 min), showing that severing activity persists in the presence of free tubulin and GTP. To our delight, severed microtubules regrew over the next several minutes, and the number of microtubules increased (Fig. 2*A*, 5, 7, and 10 min). A control mix with only tubulin, spastin, GTP, and ATP showed no de novo microtubule formation in the absence of GMP-CPP seeds, suggesting that spastin does not increase microtubule amount by promoting spontaneous nucleation. To quantify the increase in the amount of microtubule polymer in these experiments, we measured the microtubule mass on the surface over time (Fig. 2*B*, black line). Note that, because only surface-bound microtubules are observed in this assay, the total amount of polymerized tubulin is underestimated due to microtubules that dissociate from the surface and do not rebind. The surface-bound microtubule mass increased approximately exponentially during the 10 min after spastin was introduced. Fitting the growth curve with a single exponential (Fig. 2*B*, red dashed line) gave a doubling time of ∼4 min. These results show that spastin and tubulin are the minimal components sufficient to increase the total microtubule mass in vitro through a severing-dependent mechanism.

To resolve the apparent inconsistency of the observed microtubule mass increase with the GTP cap model, we investigated the fate of severed microtubule ends after cutting by spastin. The GTP cap model posits that growing microtubule ends are protected by a cap of GTP-tubulin to prevent disassembly of the unstable GDP-tubulin lattice. Therefore, the model predicts that cutting a microtubule with a severing enzyme should expose GDP-tubulin lattice at the two newly formed ends, both of which should shrink. Instead, we observed an asymmetric behavior of the new ends. Most of the newly generated plus ends depolymerized after a breakage was detected (Fig. 3*A*, yellow arrowheads). We estimated that ∼84% of the plus ends shrink (we correct for missed rescues in Fig. 3*C*) as predicted by the GTP cap model. By contrast, most of the minus ends did not shrink after severing (an example is in Fig. 3*A* with its kymograph in Fig. 3*B*; see also Movie S1) (∼80% minus ends nonshrinking), although these new minus ends can eventually be lost due to depolymerization (arrow in Fig. 3*B*). Thus, severing by spastin normally generates a new shrinking plus end and a new nonshrinking minus end.

Is modulation of microtubule dynamics necessary for the observed increase in the number and mass of microtubules? To answer this question, we extended the dynamic instability model introduced by Dogterom and Leibler (34) to include microtubule severing (Fig. 4*A*). Microtubules were considered to be in either a growing phase with growth rate $v_g$ or a shrinking phase with shrinkage rate $v_s$. Microtubules switch between these two states

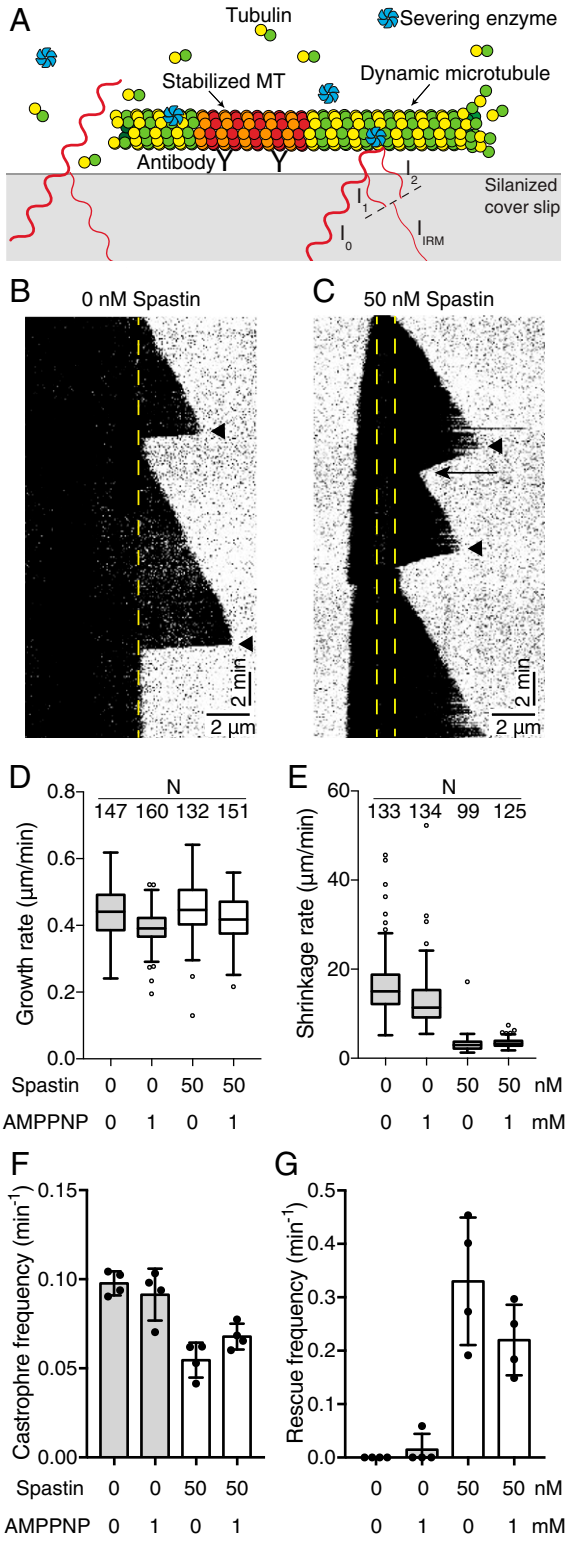


**Fig. 1.** *Drosophila* spastin modulates microtubule dynamics. (*A*) Experimental setup of the in vitro microtubule dynamic assay using IRM. The tubulin concentration was 8 µM. (*B* and *C*) Example kymographs of the dynamic microtubule assay. (*B*) Tubulin alone control with 1 mM AMP-PNP. (*C*) In the presence of 50 nM spastin + 1 mM AMP-PNP. Yellow dashed lines marked the position of GMP-CPP seeds on the kymographs. The shrinkage rate in the presence of spastin is slower than the tubulin alone control (arrowheads). A rescue event is marked with an arrow. (*D* and *E*) Comparison of growth rate and shrinkage rate in the presence of 50 nM spastin with tubulin alone control under no adenosine nucleotide and 1 mM AMP-PNP conditions. In each box, the midline shows the median value, the top and bottom lines show the 75th and 25th percentiles, and the whiskers are 1.5 interquartile ranges from the 75th and 25th percentiles. Outliers (outside the whisker range) are represented as empty circles. Sample size *N* indicates the number of microtubules analyzed in each condition. (*F* and *G*) Catastrophe and rescue frequency in the presence or absence of 50 nM spastin under no adenosine nucleotide or 1 mM AMP-PNP conditions. Error bars represent the SD. Sample size $n = 4$ independent experiments. MT, microtubule.

with catastrophe frequency $f_{gs}$ (growth to shrinkage) and rescue frequency $f_{sg}$ (shrinkage to growth) (Fig. 4*A*, rows 1 and 2). We introduced a severing rate $k$ with units of length$^{-1}$ time$^{-1}$ (Fig. 4*A*, rows 3 and 4), assuming that any position on microtubules can be severed with equal probability. Based on our experimental observations, we assumed that the newly generated plus ends shrink while the new minus ends do not. Additionally, we considered severing as a localized event that does not affect the dynamic state of the original plus ends.

An important implication of the mathematical model is that severing activity alone is not sufficient for producing more microtubules. The reason is that, when the rescue frequency is low as is the case in the absence of spastin, newly generated plus ends will depolymerize after being severed and will soon disappear. Thus, severing does not lead to a net increase in the number of microtubules, yet it causes the existing microtubules to get shorter: the total mass will, therefore, decrease. This conclusion can be made rigorous by formulating an integro-differential equation to describe the growth of microtubule mass as a function of time (*SI Appendix*). The model predicts that an increase in microtubule number and mass requires at least one of the following conditions to be satisfied: (*i*) the severing enzymes increase the number of stable seeds from which microtubules can grow, or (*ii*) the severing enzymes shift the dynamics of microtubules into their unbounded growth regime in which the average length grown is more than the length shortened ($v_g/f_{gs} > v_s/f_{sg}$) or equivalently, the net flux onto each microtubule, $(v_g f_{sg} - v_s f_{gs})/(f_{sg} + f_{gs})$, is greater than zero (34). We found that the number of stable seeds does not increase, because while the new minus ends do not shrink, they are lost when the microtubules shrink completely (Fig. 3*B* shows an arrow on the disappearing minus end) and therefore, do not serve as stable seeds. Thus, condition *i* is not met. By contrast, condition *ii* is met. The promotion of rescue events and reduction of the shrinkage rate in the presence of spastin and ATP (Table 2) lead to a reversal in sign of the net flux onto the microtubules (Table 2, row 7). Thus, switching of microtubule dynamics into the unbounded growth regime is necessary for an increase in microtubule polymer mass and number by severing.

To investigate whether rescue promotion depends on ATP hydrolysis, we directly compared the effect of spastin on microtubule dynamics in the presence of either ATP or AMP-PNP, where ATP hydrolysis is inhibited, with all other conditions identical. We found that, even in the absence of ATP hydrolysis, the rescue frequency is still significantly higher than the control (Table 2, columns 4 and 5). Moreover, the net flux in the spastin + AMP-PNP condition is larger than zero, showing that ATP hydrolysis is not necessary for the switch into the unbounded growth regime (defined above). This shows that the ATP-independent promotion of regrowth by spastin is sufficient to increase microtubule mass. Because the surface assays fail to account for dissociated microtubules, we performed microtubule spin-down assays to measure microtubule length in the bulk solution. We chemically fixed dynamic microtubules in solution with glutaraldehyde before and after incubating with spastin and sedimented the microtubules onto lysine-coated coverslips (*Materials and Methods*). Microtubules were then visualized by

**Table 1. The effects of spastin on the dynamic parameters in the absence of ATP**

| Experimental conditions | Growth rate (μm/min) | Shrinkage rate (μm/min) | Catastrophe frequency ($min^{-1}$) | Rescue frequency ($min^{-1}$) |
|---|---|---|---|---|
| Tubulin only | 0.44 ± 0.08 | 16 ± 7 | 0.098 ± 0.003 | 0 |
| 50 nM spastin | 0.45 ± 0.08 | 3.1 ± 1.7 | 0.055 ± 0.005 | 0.33 ± 0.06 |
| Tubulin + AMP-PNP | 0.39 ± 0.05 | 13 ± 6 | 0.091 ± 0.007 | 0.015 ± 0.015 |
| 50 nM spastin + AMP-PNP | 0.42 ± 0.07 | 3.4 ± 0.9 | 0.068 ± 0.004 | 0.22 ± 0.03 |

Dynamic assay data at 8 μM tubulin from Fig. 1 were collected from four independent experiments for each condition. The values shown are mean ± SD. Total numbers of rescues observed in each condition are 0, 56, 1, and 39.

direct immunofluorescence. Similar to the surface assay, the spin-down assay showed that the microtubule number and density increased in the bulk in the presence of spastin (Fig. 4*B*, *Upper*). In these experiments, we observed microtubule bundles as has been seen for human spastin (35, 36). Spastin had a pronounced effect on the microtubule length distribution. The steady-state length distribution in the absence of spastin was close to an exponential distribution as predicted by the model of Dogterom and Leibler (34) (Fig. 4*B*, *Lower Left*). Ten minutes after introducing 50 nM spastin, the mean length was shorter (5.5–4.0 μm), and the length distribution was narrower (SD decreased from 4.4 to 2.1 μm) and peaked (Fig. 4*B*, *Lower Right*), analogous to the predictions from previous mathematical models of actin filament severing (37) and microtubule severing (38). Thus, *Drosophila* spastin gives rise to a larger microtubule mass by a steady increase in the number of shorter microtubules.

To investigate the molecular mechanism of spastin-mediated regulation of microtubule dynamics, we visualized the interaction between fluorescently labeled spastin and dynamic microtubules with time-lapse TIRF microscopy and IRM. In the absence of adenosine nucleotide or with 1 mM AMP-PNP, we found that spastin accumulates with high local density at the shrinking microtubule plus ends (Fig. 5*A*). Similar signal foci corresponding to spastin accumulation were also detected in IRM. These distinct foci dwell at the microtubule ends and follow the tips during the shrinkage process (Fig. 5 *A* and *B*, kymograph and Movie S2). In these experiments, slower shrinkage rates and increased rescue frequency were also observed, consistent with experiments using unlabeled spastin. During the microtubule growth phase, spastin binds along the microtubule shaft, but no obvious tip tracking or tip accumulation was seen (first frame in Fig. 5*A*, *Right* and kymograph in Fig. 5*B*, *Upper*). Furthermore, we tested if spastin also follows the shrinking microtubule tip in the presence of ATP, which is required for severing activity. After perfusing in the reaction mix containing fluorescently labeled spastin, unlabeled tubulin, GTP, and ATP, fluorescent signals appeared along the microtubules, and severing events quickly occurred. Similar to the no ATP and AMP-PNP conditions, foci containing high density of spastin resided at the shrinking plus ends generated from severing or catastrophe events and remained associated with the shrinking tips during shortening (an example is in Fig. 5 *C*, red arrows and *D*, red arrowheads; see also Movie S3). Analysis of the time course of the intensity increase showed that the accumulation typically happens over the first 10–15 s after shrinkage in the presence of ATP (*SI Appendix*, Fig. S5). Interestingly, the fluorescent signal of spastin at the GMP-CPP microtubule regions (center part in Fig. 5 *A* and *C*) is much weaker than the one at the GDP microtubule extension with or without ATP, suggesting that spastin may preferentially bind to the GDP lattice and thus, lessen the cutting at the microtubule ends. Together, our data demonstrate that spastin preferentially binds and tracks the shrinking microtubule ends independent of ATP hydrolysis.

## Discussion

We discovered that *Drosophila* spastin and tubulin are the minimal protein components sufficient to increase microtubule number and total polymer mass by combining severing activity with modulation of microtubule dynamics. Before accepting this conclusion, we addressed a number of potential caveats that may

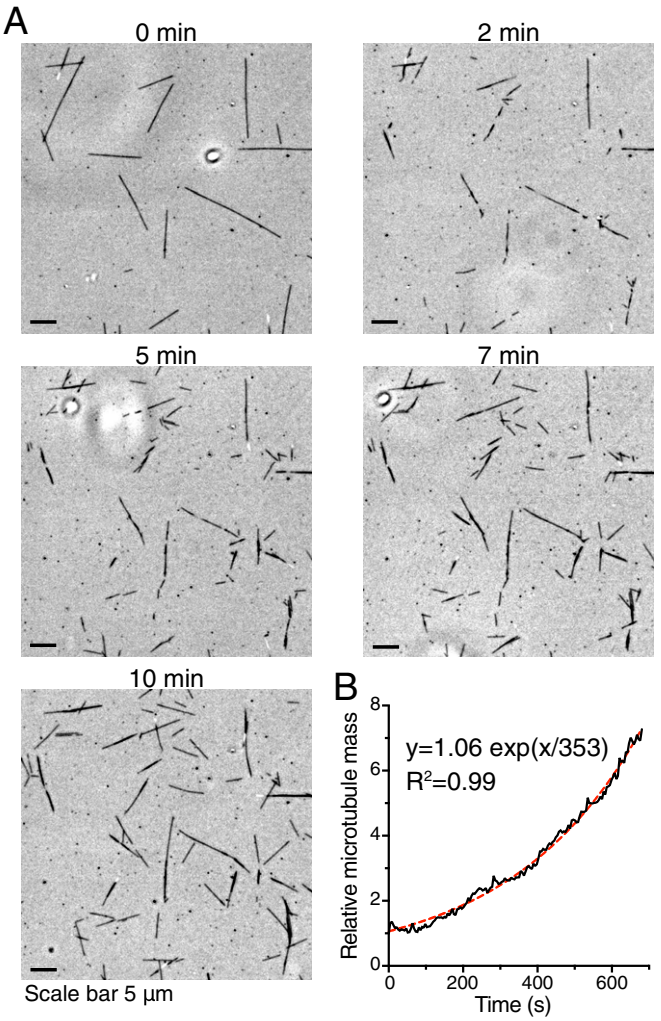


**Fig. 2.** Spastin severs dynamic microtubules and increases the total mass and number of microtubules. (*A*) Time series of dynamic microtubules severed and amplified by spastin using IRM imaging. Breakage and regrowth of microtubules occurred when treated with 50 nM spastin and 1 mM ATP. (*B*) Example of total microtubule mass increasing over time in the dynamic microtubule-severing assay. The black line shows the relative total microtubule mass normalized by time = 0 s. The increase of total microtubule mass was fitted by a single-exponential growth curve (red dashed line).

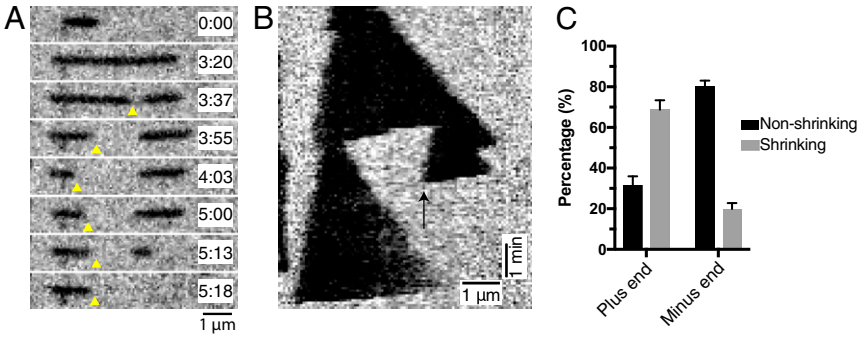


**Fig. 3.** Asymmetric behaviors of the two microtubule ends generated after severing. (*A*) Representative time series of dynamic severed microtubule. The corresponding kymograph is in *B*. The microtubule plus end is to the right. After the breakage occurred, the newly generated plus end (yellow arrowheads) shrank and rescued, while the new minus end directly regrew without detectable shrinkage taking place. (*C*) Quantification of the percentages of nonshrinking and shrinking ends generated by severing. The majority of new plus ends shrank after cut (mean ± SD; 69 ± 5%), and newly generated minus ends are mostly nonshrinking (80 ± 3%). Measurements were quantified from four independent experiments. The probability of a shrinking plus end rescuing within 0.5 μm (the shrinking length that can be confidently measured) is ∼15%, which was estimated from the rescue frequency and shrinkage rate measured in Table 2, assuming that rescue is a Poisson process. The error-corrected percentage of shrinking plus end is, therefore, 84%.

impact its validity. First, the increase in microtubule number and mass was not caused by polymerization from severed GMP-CPP microtubule fragments, because most of the newly generated microtubules lack fluorescence signal from the labeled seeds in our dynamic microtubule-severing assay (*SI Appendix*, Fig. S3). Second, the increase in microtubule number was not due to surface binding artifacts leading to biased sampling in our flow channel assay, because we confirmed that spastin can increase microtubule density in solution using a microtubule spin-down assay (Fig. 4*B*). The increase in microtubule polymer mass was not a result of spontaneous, de novo nucleation, because this would lead to a linear increase in microtubule number, not the observed exponential increase, as expected if each spastin-induced cut led to two new microtubules. Another argument against spontaneous nucleation is that there was no observed de novo nucleation with only spastin, GTP, ATP, and tubulin at the concentration that we used, and spastin has only modest effects on the microtubule growth and catastrophe rates. Therefore, none of these caveats are likely to apply.

We conclude, therefore, that spastin increases microtubule mass by using its severing activity to create new microtubules that can serve as templates to support new microtubule growth as hypothesized by earlier works to explain the cellular phenotypes (19, 22, 23). These dual functions of spastin—severing and promotion of regrowth—lead to autocatalytic microtubule assembly. Thus, spastin has some functional similarities to augmin (39), which gives rise to autocatalytic microtubule growth through a branching rather than severing mechanism (40).

**Molecular Mechanism of Microtubule Dynamics Regulation by Spastin.** The key functional properties of spastin, in addition to the severing activity, are the slowing down of microtubule shrinkage and the promotion of rescue. In this way, microtubule dynamics switches from bounded to unbounded growth, which we showed using our mathematical model to be essential for the nucleation-like activity. What is the molecular mechanism behind spastin regulating shrinkage and rescue? A recent study of microtubule severases has suggested that the incorporation of

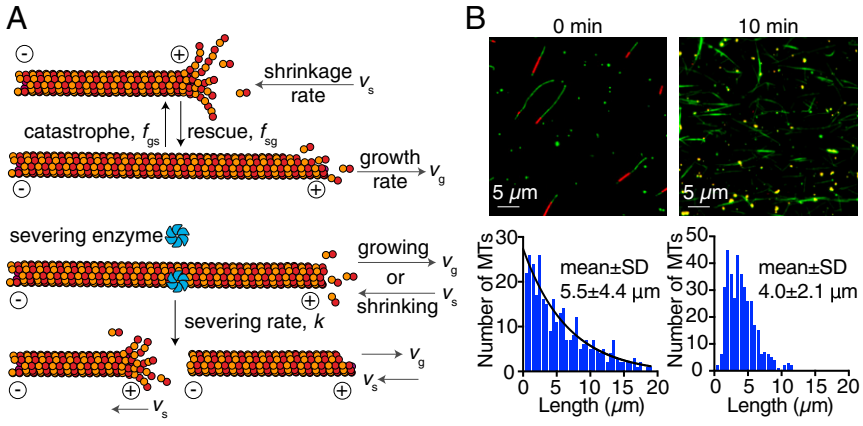


**Fig. 4.** Mathematical model and microtubule length distribution. (*A*) Graphic representation of the dynamic instability with severing model. Rows 1 and 2 correspond to the canonical dynamic instability model. Rows 3 and 4 show that, when a microtubule is severed, the newly generated plus end starts shrinking. Here, we considered all of the minus ends as "neutral" ends where no growth or shrinkage takes place but that will disappear after the microtubules depolymerize completely. (*B*) Bulk measurement of microtubule length in the presence of severing with microtubule spin-down assay. *Upper* shows the example epifluorescence images before and 10 min after initiating severing reaction. Red indicates TAMRA-labeled GMP-CPP microtubule seeds. Green indicates tubulin (Alexa-488–labeled antitubulin antibody). Microtubule density increased notably 10 min after introducing 50 nM spastin. *Lower* shows the length distribution of 0 min (*Left*) and 10 min (*Right*) after the severing reaction. Severing shortens the mean length and changes the distribution from an exponential-like to a more compact peak-like function. The black line in *Left* indicates the exponential fit. Mean lengths ± SD: 5.5 ± 4.4 μm (0 min) and 4.0 ± 2.1 μm (10 min). Numbers of microtubules measured: 319 (0 min) and 377 (10 min). MT, microtubule.

**Table 2. The effects of spastin on the dynamic parameters in the presence of ATP compared with the effects in AMP-PNP**

| Dynamics parameters | Tubulin control | 50 nM spastin + ATP | Tubulin control + AMP-PNP | 50 nM spastin + AMP-PNP |
|---|---|---|---|---|
| Growth rate, $v_g$, μm/min | 0.71 ± 0.12 | 0.79 ± 0.15 | 0.70 ± 0.12 | 0.70 ± 0.13 |
| Shrinkage rate, $v_s$, μm/min | 15.8 ± 5.1 | 9.9 ± 4.3 | 19.8 ± 8.0 | 5.1 ± 2.6 |
| Catastrophe frequency, $f_{gs}$, $min^{-1}$ | 0.098 ± 0.02 | (0.098 ± 0.02) | 0.11 ± 0.01 | 0.054 ± 0.017 |
| Rescue frequency, $f_{sg}$, $min^{-1}$ | 0.43 ± 0.13 | 3.12 ± 0.45 | 0.19 ± 0.08 | 1.36 ± 0.25 |
| Probability of rescue | 9.8 ± 3.2% | 73.0 ± 6.1% | 3.6 ± 1.9% | 85.4 ± 8.9% |
| Average flux $(v_g f_{sg} - v_s f_{gs})/(f_{gs} + f_{sg})$, μm/min | −2.35 | +0.46 | −6.82 | +0.48 |

Microtubule dynamics were measured in the presence of spastin severing and in the presence of the nonhydrolyzable ATP analog AMP-PNP with 12 μM tubulin. The catastrophe frequency in the presence of spastin and ATP was not quantified due to the severing of microtubules taking place in the experiments. The catastrophe frequency quantified from control experiments was used to calculate the average flux for the case of spastin + ATP. The probability of rescue is defined as the number of rescue events divided by the number of shrinkage events. Number of microtubules analyzed: 78 (ATP control), 82 (ATP + spastin), 113 (AMP-PNP control), and 133 (AMP-PNP + spastin) from three independent experiments. The values shown are mean ± SD of the triplicates. Total numbers of rescues observed in each condition are 9, 63, 7, and 103.

GTP-tubulin–like islands into damaged sites generated by severing enzymes can promote rescues of the microtubules and increase total microtubule numbers (25). However, we discovered that a significant increase in the rescue frequency and slowing of the shrinkage rate were still observed in the absence of adenosine nucleotide or in the presence of AMP-PNP (Fig. 1 *B* and *C* and Table 2), conditions under which neither severing nor lattice damage occur (25). To exclude the possibility of experimental variations, we performed additional control experiments measuring spastin's effects on microtubule dynamics in the presence of ATP or AMP-PNP on the same day under identical conditions. The rescue frequencies were 3.46 ± 0.58 and 1.53 ± 0.24 $min^{-1}$ (mean ± SE) for spastin + ATP and spastin + AMP-PNP conditions, respectively, which are consistent with our previous measurements in Table 2. Our results, therefore, demonstrate that spastin can promote rescue even when the ATP hydrolysis is inhibited and the lattice damage generated by spastin is absent. This suggests that spastin can promote microtubule rescue through a mechanism that does not involve self-repairing of damage and that GTP-tubulin incorporation into the microtubule lattice may be dispensable for the nucleation-like activity of microtubule severases.

Our time-lapse TIRF microscopy experiments provide an alternative mechanism for the effect of spastin on microtubule dynamics: accumulation and tracking of spastin molecules at the shrinking microtubule plus ends, which we observed under all

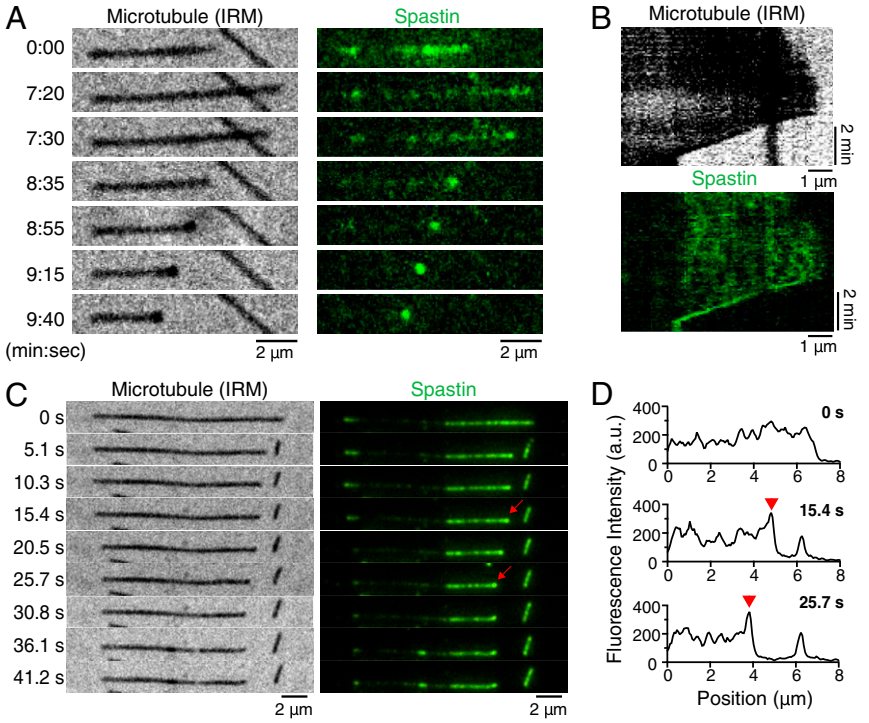


**Fig. 5.** *Drosophila* spastin tracks and concentrates on shrinking microtubule tips. (*A*) Representative time series showing that DyLight488-labeled spastin (shown in green) accumulates and remains associated with a microtubule plus end during shrinkage in the absence of ATP. Microtubules were visualized by IRM, and fluorescent spastin molecules were imaged by TIRF microscopy. Distinct foci were visible in both IRM and TIRF channels. Corresponding kymographs are shown in *B*. (*C*) Example time series of spastin molecules accumulating at a shrinking microtubule tip in the presence of 1 mM ATP. High-intensity foci localize at the shrinking plus end generated by severing (red arrows). Shrinkage stops in the last three frames, presumably due to a rescue event. The middle region, where the spastin signal is weak, corresponds to the GMP-CPP microtubule seed. (*D*) Line-scan fluorescence intensity profile of dynamic microtubule segments from *C* showing a high signal peak (red arrowheads) that corresponds to the high density of spastin that accumulates at the shrinking microtubule tip. Plus ends of microtubules are all pointing to the right.

adenosine nucleotide conditions (ATP, AMP-PNP, and no adenosine nucleotide). We, therefore, propose that spastin can slow down microtubule shortening and promote rescue through multivalent interactions with shortening microtubule tips, which slows depolymerization of the GDP-tubulin lattice sufficiently to allow another GTP-tubulin cap to become established (Fig. 6). Similar mechanisms have been proposed for the interaction of shrinking microtubule ends with the Dam1 and Ndc80 complexes to facilitate kinetochore microtubule attachment; both can decrease the microtubule shrinkage rate and increase rescue frequency (41–43). Spastin molecules can potentially cross-link adjacent tubulin dimers. Cross-linking along the protofilament is then expected to slow down dissociation of the dimer from the end. Cross-linking between protofilaments is expected to inhibit peeling, which in turn, would slow depolymerization. While it is easy to understand why accumulation of spastin would lead to a slowdown of shrinkage, it is more difficult to reconcile the slowdown with the subunit exchange/GTP island mechanism, because this mechanism predicts unchanged shrinkage speed until the island is reached.

Considering the high sequence and functional conservation, it is expected that the other microtubule severases, katanin and fidgetin, have similar activities to spastin. Similar to the case of katanin (28), we observed that free tubulin reduces the microtubule binding affinity of spastin (*SI Appendix*, Fig. S4) and thus, greatly increases the spastin concentration required for severing dynamic microtubules, therefore increasing microtubule number (e.g., while severing occurs at 50 nM spastin, it is very slow at 35 nM spastin). Katanin has been shown to decorate and depolymerize microtubules at both ends (29, 44). While we observed that spastin preferentially binds and tracks the shrinking microtubule plus ends, we did not observe notable end depolymerization activity for spastin in any of the concentrations that we tested (~1 nM to 4 μM). The molecular basis behind these disparities remains unclear, and additional biochemical and structural studies are needed to provide more insight into these differences between spastin and katanin.

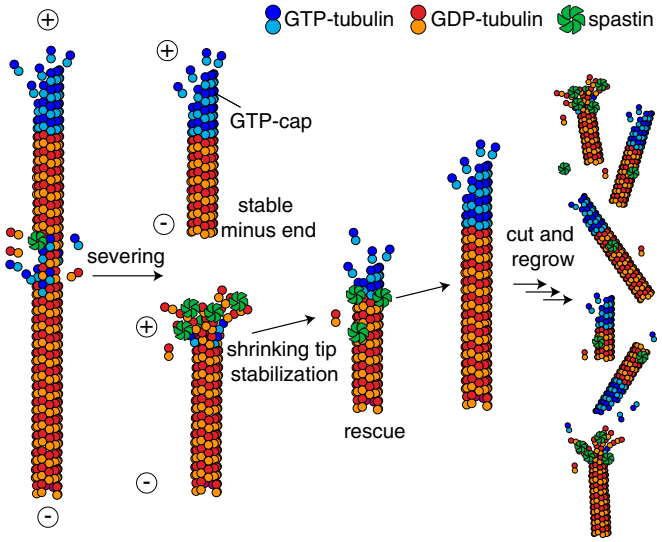


**Fig. 6.** Proposed model for increasing microtubule polymer mass by spastin. Tubulin subunits are removed from the microtubule lattice by spastin and lead to severing. Spastin molecules accumulate on the shrinking microtubule plus ends, potentially stabilizing the shrinking tip, and thus, they reduce the shrinkage rate and increase the rescue frequency. The promotion of rescue and slowdown of shrinkage lead to an increase in net flux onto the microtubules. When the average net flux becomes positive (unbounded growth regime), microtubule number and mass are increased by severing.

Another interesting observation is the asymmetric fate of newly generated microtubule ends after severing by spastin. We found that the new plus ends, consistent with the GTP cap model, are mostly in the shrinking phase. This finding is consistent with the observations in plant cells (45) but is not in agreement with Vemu et al. (25), who found that most of the new plus ends were in the growing phase. A possible explanation for the discrepancy is that Vemu et al. (25) failed to correct for missed rescues that would reduce the number of shrinking events observed. This underestimation may be as large as 25%, considering rescue as a Poisson process. The stability of the new plus end has important implications with respect to the different models, because the subunit exchange mechanism predicts that the newly generated plus end will be stable if the cut occurs in the middle of the GTP island. Thus, more detailed study of spastin localization will be important.

The new minus ends, in contrast to plus ends, are mostly in the growth phase without significant shortening. This observation is curious: it seems to be inconsistent with the GTP cap model, because the exposed GDP lattice should shrink. However, the observation matches the results in early studies using UV lasers and glass microneedles to sever dynamic microtubules in vitro (46, 47). Given that this asymmetric behavior was observed in both mechanical and protein-induced severing raises the possibility that the two ends may be inherently different in terms of their GTP-tubulin caps and stability. One possible model is that the microtubule minus end with exposed GDP-tubulin can exist in two states with different stability: an unstable end that will depolymerize, and a stable end that can add GTP-tubulin to form a cap, which leads to growth. If the stable end is more prevalent than the unstable one, then severing will usually produce a stable minus end. The finding that Op18/stathmin differentially regulates catastrophe at the two ends suggests that there might be structural differences between the plus and minus ends (48, 49). Our understanding of the nature of microtubule minus ends is still very limited, and it remains an important topic to explore.

**Are Severases Microtubule Network Assemblers or Disassemblers?** Severing enzymes were first proposed to facilitate the disassembly of cellular microtubules networks in sea urchin embryos (7) and disintegration of flagella in *Chlamydomonas* (50). This proposal was subsequently supported by studies showing that overexpression of spastin and katanin in cultured cells reduced the number of cellular microtubules (33, 51). Consistent with these findings, RNAi knockdown of spastin increases the number of stable microtubules (18), and inhibition of katanin leads to an increase in the size of mitotic spindles in *Xenopus* egg extracts (52). However, in vivo work on spastin and katanin suggested a possible nucleation-like and microtubule assembly activity for microtubule severases (16, 19–21). Our in vitro studies on spastin directly show that this protein has nucleation-like and microtubule network assembly activity. Indeed, if katanin behaves similarly in sea urchin embryos, then it may be involved not only in disassembling the interphase microtubules as originally thought (53) but also, in their assembly.

Severing enzymes have been proposed to both promote and antagonize microtubule assembly. Here, we propose a hypothesis that can potentially reconcile contradicting phenotypes. Our mathematical model predicts that the boundary between bounded and unbounded growth, which is determined by the microtubule dynamics parameters, serves as a threshold for whether severing is destructive or productive. Many microtubule-associated proteins alter the parameters of microtubule dynamics (54) and will, therefore, affect this threshold. Thus, the presence of other microtubule dynamics regulators is expected to have a significant impact on the effect of microtubule severing. An important example of regulation of microtubule-associated protein activity occurs in the cell cycle. For example, when

*Xenopus* egg extracts enter metaphase, microtubule dynamics shifts from the unbounded to bounded growth as a consequence of cyclin B-dependent catastrophe promotion (55). This change in dynamics can potentially couple with the severing activity to efficiently disintegrate the interphase microtubule network before spindle assembly at mitotic entry (53). Thus, the threshold between bounded and unbounded growth serves as a control parameter: crossing the threshold (for example, through the action of a microtubule-associated protein) switches the system from disassembly to assembly. Because assembly is autocatalytic, additional mechanisms to switch it off will be essential.

We have demonstrated that *Drosophila* spastin itself possesses the long-postulated microtubule nucleation-like activity and can increase the overall microtubule number and density by alteration of dynamic instability. An important implication is that severases can promote acentrosomal microtubule formation in systems, such as neurons, animal oocytes, and plant cells, where microtubule organization centers are distant or absent (11, 14, 19, 23). Other microtubule stabilizers, especially rescue factors, such as CLIPs and CLASPs (45, 56, 57), can potentially further amplify the nucleation-like effect of microtubule severases or decrease the tubulin concentration needed by stabilizing the newly severed plus ends. Interestingly, severing proteins are crucial for both aligning *Arabidopsis* cortical microtubule arrays (13, 14, 58) and neuronal branching morphogenesis (15, 17, 21, 59, 60). The microtubule organization of these two processes is distinctively different. Microtubules in plant cortical arrays are highly parallel, while those at the dendritic branches are presumably angled. These morphological differences of microtubule organization may arise from the differential participations of other microtubule-associated proteins, such as augmin-γ-TuRC complex, motors, and dynamic regulators with microtubule severing. It will be of great interest to understand how different microtubule-associated proteins can collectively modulate microtubule generation and dynamic instability to provide the versatility of microtubule severases and regulate the complex cellular microtubule networks.

## Materials and Methods

**Protein Preparation.** Bovine brain tubulin was purified and labeled with carboxytetramethylrhodamine-*N*-hydroxysuccinimidyl ester (TAMRA-NHS) (Thermofisher) according to the previously described protocol (61, 62). Stabilized microtubule seeds were polymerized with GMP-CPP (Jena Bioscience) following the method described previously (63). *Drosophila melanogaster* spastin short isoform (208-aa end) with an N-terminal KKCK tag for fluorescently labeling was cloned into pET vector with N-terminal $His_6$–maltose-binding protein (MBP) tag using ligation-independent cloning. pET His6 MBP TEV LIC cloning vector (1 M) was a gift from Scott Gradia, University of California, Berkeley, CA (Addgene plasmid 29656). *Drosophila* spastin tagged with $His_6$-MBP was expressed in *Escherichia coli* (Rosetta-DE3–competent cells; Novagen) overnight at 16 °C. *E. coli* cells were first resuspended in cold lysis buffer [30 mM Hepes, pH 7.4, 0.3 M NaCl, 10 mM imidazole, 5% glycerol, 2 mM DTT, 10 μM ATP, protease inhibitors (0.2 mM pefabloc, 5 μg/mL leupeptin), 0.3 U/μL bezonase] and sonicated on ice to break the cells. The crude lysate was clarified and loaded onto a His-tagged protein purification column (GE-Healthcare), and it was washed with imidazole buffer (30 mM Hepes, pH 7.4, 0.3 M NaCl, 5% glycerol, 50 mM imidazole, 2 mM DTT, 10 μM ATP). The protein was then eluted with continuous gradient elution (50 mM to 375 mM imidazole). Peak fractions were pooled and diluted with MBP binding buffer (30 mM Hepes, 0.3 M NaCl, 5 mM $MgSO_4$, 2 mM DTT, 10 μM ATP) to imidazole concentration less than 50 mM. The solution was then loaded on dextrin-Sepharose column (GE-Healthcare), washed with MBP binding buffer, and eluted with 10 mM maltose. The eluted protein was first diluted with dialysis buffer (30 mM Hepes, pH 7.4, 0.2 M KCl, 5 mM $MgSO_4$, 10% glycerol, 0.2% 2-mercaptoethanol, 10 μM ATP) to protein concentration lower than 2 mg/mL, was dialyzed, and cleaved the tag with TEV-protease (Sigma) overnight at 4 °C. The uncleaved spastin and cleaved $His_6$-MBP were then removed by passing through His column. The flow through was then further purified and buffer exchanged to elution buffer Brinkley reassembly buffer (BRB80) [80 mM piperazine-*N*,*N*′-bis(2-ethanesulfonic acid) (PIPES), pH 6.9, 1 mM EGTA, 1 mM $MgCl_2$], 200 mM KCl, 10 μM ATP, and 0.5 mM Tris(2-carboxyethyl)phosphine (TCEP) with size exclusion column (Superdex 200; GE-Healthcare). The peak fractions were pooled, concentrated, flash frozen with liquid nitrogen, and stored in −80 °C.

For fluorophore labeling, purified spastin was treated with 1 mM TCEP in BRB80 + 150 mM KCl on ice for 20 min to reduce the thiol group of cysteine. DyLight488-maleimide (Thermofisher) was added to spastin in a 10:1 molar ratio and incubated at 4 °C for 2 h in the dark. Free fluorescent dye was removed by the dye removal column (Pierce) according to the manufacturer's instruction. Fluorescently labeled spastin was then buffer exchanged with spin-desalting column (Thermofisher) into BRB80 + 200 mM KCl + 0.1% 2-mercaptoethanol.

**Microtubule Dynamic Assay and Imaging Condition.** Microtubule dynamic assay was done similar to the previously described method (63), with the exception that the imaging was done by IRM for unlabeled microtubules as formerly described (30). The imaging buffer consisted of BRB80 supplemented with 50 mM KCl, 1 mM $MgCl_2$, and 5 mM DTT for IRM imaging. The microtubule dynamic assay was performed with 1 mM GTP, 8 μM tubulin, and 50 nM spastin with or without 1 mM AMP-PNP at 28 °C. Observation of fluorescent spastin on dynamic microtubule in the absence of adenosine nucleotide or with 1 mM AMP-PNP was performed similarly using 50 nM DyLight-488 spastin with unlabeled tubulin, supplemented with oxygen scavenger mix (40 mM glucose, 40 mg/mL glucose oxidase, 16 mg/mL catalase, 0.1 mg/mL casein, 10 mM DTT), and imaged by TIRF microscopy with 488-nm excitation light and IRM.

**Dynamic Microtubule Severing Assay.** Dynamic microtubule-severing assay was performed similarly to microtubule dynamic assay, with the exception that higher concentration of antitubulin antibody (clone SAP.4G5; Sigma) or truncated kinesin rigor mutant (rat Kif5c-430 G235A) was used to affix the microtubules onto the surface to retain the cut microtubules from rapid detachment. The imaging buffer consisted of BRB80, 1 mM $MgCl_2$, 50 mM KCl, 1 mM GTP, 1 mM ATP supplemented with 40 mM glucose, 40 mg/mL glucose oxidase, 16 mg/mL catalase, 0.1 mg/mL casein, and 10 mM DTT. Microtubules were imaged with both IRM and TIRF microscopy, with an average frame rate of 0.23 frames per second (fps); 12 μM unlabeled tubulin with imaging buffer was first introduced to the flow chamber to grow dynamic microtubules from TAMRA-labeled GMP-CPP seeds for 15 min. Severing reaction mix containing 50 nM spastin, 12 μM unlabeled tubulin, and imaging buffer was then flowed into the flow chamber to observe the severing and dynamics of microtubules at 28 °C. Observation of fluorescent spastin distribution on microtubule ends in the presence of 1 mM ATP was performed similarly with 50 nM Dylight 488-spastin and imaged by IRM, TIRF (488-nm excitation), and TIRF (561-nm excitation), with the average frame rate of 0.19 fps.

**Microtubule Spin-Down Assay.** Severing reaction was done similar to the flow channel dynamic microtubule-severing assay. In brief, TAMRA-labeled GMP-CPP microtubules were incubated with 12 μM bovine tubulin (unlabeled), 1 mM GTP, 1 mM MgATP, 50 mM KCl, and 5 mM DTT in BRB80 at 28 °C to grow dynamic microtubules from the seeds for 20 min. Spastin was then introduced with the final concentration of 50 nM. Microtubule solutions were fixed at different time points by diluting to 30 times volume fixation solution (1% glutaraldehyde, 1 mM AMP-PNP in BRB80) and incubated at room temperature for 2 min. The fixed reactions were then diluted 30 times with BRB80 and quenched with 50 mM $NH_4Cl$. Microtubule solution was then laid on top of a 35% glycerol-BRB80 cushion and spun down to the polylysine-treated 8-mm round coverslips in a Beckman TLS-55 swinging bucket rotor at 35,000 rpm for 20 min. The coverslips were then blocked with 2 mg/mL casein followed by incubation with 1:500 Alexa-488–labeled anti–α-tubulin antibody (clone DM1A; EMD Millipore) and visualized by epifluorescence.

**Image Analysis.** Kymographs of individual microtubules were created with ImageJ software (NIH) to measure the microtubule dynamics. Growth rates and shrinkage rates were measured from the ratio of horizontal and vertical distances from the kymographs. Catastrophe frequency was determined by the total number of catastrophe events divided by the total growth time. Similarly, rescue frequency was determined by the number of rescues observed divided by total shrinkage time. Lengths of microtubules were measured with ImageJ. Drift correction of movies was performed by using the template-matching ImageJ plugin (64). In the case of the dynamic microtubule-severing assay, movies from the IRM channel were first thresholded. TIRF channel images were used as a mask to remove the GMP-CPP microtubules. The relative total microtubule mass in dynamic severing assay was then measured using the ImageJ built-in Analyze Particles algorithm and normalized by the first frame. For microtubule length distribution measurement in

the spin-down assay, only microtubules with both ends clearly identified were measured. Microtubules with significant overlap or bundling were excluded from the length measurement.

**Data Availability Statement.** Additional data that support the findings of this study are available in the *SI Appendix*.

**ACKNOWLEDGMENTS.** We thank the current and previous members of the laboratory of J.H. for the discussions on the manuscript. We thank the Sindelar laboratory for constructive advice and feedback on the manuscript draft and the De La Cruz laboratory for sharing the swing-bucket ultracentrifuge rotor. Y.-W.K. was supported by a fellowship from the Ministry of Education in Taiwan. This work was supported by NIH Grants R01 GM110386 (to J.H.) and DP1 M110065 (to J.H.).

1. Kirschner M, Mitchison T (1986) Beyond self-assembly: From microtubules to morphogenesis. *Cell* 45:329–342.
2. Desai A, Mitchison TJ (1997) Microtubule polymerization dynamics. *Annu Rev Cell Dev Biol* 13:83–117.
3. Howard J, Hyman AA (2003) Dynamics and mechanics of the microtubule plus end. *Nature* 422:753–758.
4. Mitchison T, Kirschner M (1984) Dynamic instability of microtubule growth. *Nature* 312:237–242.
5. Drechsel DN, Kirschner MW (1994) The minimum GTP cap required to stabilize microtubules. *Curr Biol* 4:1053–1061.
6. Maurer SP, Bieling P, Cope J, Hoenger A, Surrey T (2011) GTPgammaS microtubules mimic the growing microtubule end structure recognized by end-binding proteins (EBs). *Proc Natl Acad Sci USA* 108:3988–3993.
7. McNally FJ, Vale RD (1993) Identification of katanin, an ATPase that severs and disassembles stable microtubules. *Cell* 75:419–429.
8. Howard J, Hyman AA (2007) Microtubule polymerases and depolymerases. *Curr Opin Cell Biol* 19:31–35.
9. Roll-Mecak A, McNally FJ (2010) Microtubule-severing enzymes. *Curr Opin Cell Biol* 22:96–103.
10. Zhang D, Rogers GC, Buster DW, Sharp DJ (2007) Three microtubule severing enzymes contribute to the "Pacman-flux" machinery that moves chromosomes. *J Cell Biol* 177:231–242.
11. McNally K, Audhya A, Oegema K, McNally FJ (2006) Katanin controls mitotic and meiotic spindle length. *J Cell Biol* 175:881–891.
12. Rasi MQ, Parker JDK, Feldman JL, Marshall WF, Quarmby LM (2009) Katanin knockdown supports a role for microtubule severing in release of basal bodies before mitosis in Chlamydomonas. *Mol Biol Cell* 20:379–388.
13. Nakamura M, Ehrhardt DW, Hashimoto T (2010) Microtubule and katanin-dependent dynamics of microtubule nucleation complexes in the acentrosomal Arabidopsis cortical array. *Nat Cell Biol* 12:1064–1070.
14. Lindeboom JJ, et al. (2013) A mechanism for reorientation of cortical microtubule arrays driven by microtubule severing. *Science* 342:1245533.
15. Ahmad FJ, Yu W, McNally FJ, Baas PW (1999) An essential role for katanin in severing microtubules in the neuron. *J Cell Biol* 145:305–315.
16. Sherwood NT, Sun Q, Xue M, Zhang B, Zinn K (2004) Drosophila spastin regulates synaptic microtubule networks and is required for normal motor function. *PLoS Biol* 2:e429.
17. Jinushi-Nakao S, et al. (2007) Knot/Collier and cut control different aspects of dendrite cytoskeleton and synergize to define final arbor shape. *Neuron* 56:963–978.
18. Trotta N, Orso G, Rossetto MG, Daga A, Broadie K (2004) The hereditary spastic paraplegia gene, spastin, regulates microtubule stability to modulate synaptic structure and function. *Curr Biol* 14:1135–1147.
19. Srayko M, O'toole ET, Hyman AA, Müller-Reichert T (2006) Katanin disrupts the microtubule lattice and increases polymer number in C. elegans meiosis. *Curr Biol* 16:1944–1949.
20. Wood JD, et al. (2006) The microtubule-severing protein Spastin is essential for axon outgrowth in the zebrafish embryo. *Hum Mol Genet* 15:2763–2771.
21. Stewart A, Tsubouchi A, Rolls MM, Tracey WD, Sherwood NT (2012) Katanin p60-like1 promotes microtubule growth and terminal dendrite stability in the larval class IV sensory neurons of Drosophila. *J Neurosci* 32:11631–11642.
22. Roll-Mecak A, Vale RD (2006) Making more microtubules by severing: A common theme of noncentrosomal microtubule arrays? *J Cell Biol* 175:849–851.
23. Kapitein LC, Hoogenraad CC (2015) Building the neuronal microtubule cytoskeleton. *Neuron* 87:492–506.
24. Roostalu J, Surrey T (2017) Microtubule nucleation: Beyond the template. *Nat Rev Mol Cell Biol* 18:702–710.
25. Vemu A, et al. (2018) Severing enzymes amplify microtubule arrays through lattice GTP-tubulin incorporation. *Science* 361:eaau1504.
26. Dimitrov A, et al. (2008) Detection of GTP-tubulin conformation in vivo reveals a role for GTP remnants in microtubule rescues. *Science* 322:1353–1356.
27. Tropini C, Roth EA, Zanic M, Gardner MK, Howard J (2012) Islands containing slowly hydrolyzable GTP analogs promote microtubule rescues. *PLoS One* 7:e30103.
28. Bailey ME, Sackett DL, Ross JL (2015) Katanin severing and binding microtubules are inhibited by tubulin carboxy tails. *Biophys J* 109:2546–2561.
29. Jiang K, et al. (2017) Microtubule minus-end regulation at spindle poles by an ASPM-katanin complex. *Nat Cell Biol* 19:480–492.
30. Mahamdeh M, Simmert S, Luchniak A, Schäffer E, Howard J (2018) Label-free high-speed wide-field imaging of single microtubules using interference reflection microscopy. *J Microsc* 272:60–66.
31. Solowska JM, et al. (2008) Quantitative and functional analyses of spastin in the nervous system: Implications for hereditary spastic paraplegia. *J Neurosci* 28:2147–2157.
32. Itzhak DN, Tyanova S, Cox J, Borner GH (2016) Global, quantitative and dynamic mapping of protein subcellular localization. *eLife* 5:570.
33. Roll-Mecak A, Vale RD (2005) The Drosophila homologue of the hereditary spastic paraplegia protein, spastin, severs and disassembles microtubules. *Curr Biol* 15:650–655.
34. Dogterom M, Leibler S (1993) Physical aspects of the growth and regulation of microtubule structures. *Phys Rev Lett* 70:1347–1350.
35. Salinas S, et al. (2005) Human spastin has multiple microtubule-related functions. *J Neurochem* 95:1411–1420.
36. Eckert T, Le DT-V, Link S, Friedmann L, Woehlke G (2012) Spastin's microtubule-binding properties and comparison to katanin. *PLoS One* 7:e50161.
37. Ermentrout GB, Edelstein-Keshet L (1998) Models for the length distributions of actin filaments. II. Polymerization and fragmentation by gelsolin acting together. *Bull Math Biol* 60:477–503.
38. Tindemans SH, Mulder BM (2010) Microtubule length distributions in the presence of protein-induced severing. *Phys Rev E Stat Nonlin Soft Matter Phys* 81:031910.
39. Goshima G, Mayer M, Zhang N, Stuurman N, Vale RD (2008) Augmi. A protein complex required for centrosome-independent microtubule generation within the spindle. *J Cell Biol* 181:421–429.
40. Petry S, Groen AC, Ishihara K, Mitchison TJ, Vale RD (2013) Branching microtubule nucleation in Xenopus egg extracts mediated by augmin and TPX2. *Cell* 152:768–777.
41. Franck AD, et al. (2007) Tension applied through the Dam1 complex promotes microtubule elongation providing a direct mechanism for length control in mitosis. *Nat Cell Biol* 9:832–837.
42. Westermann S, et al. (2006) The Dam1 kinetochore ring complex moves processively on depolymerizing microtubule ends. *Nature* 440:565–569.
43. Volkov VA, Huis In 't Veld PJ, Dogterom M, Musacchio A (2018) Multivalency of NDC80 in the outer kinetochore is essential to track shortening microtubules and generate forces. *eLife* 7:576.
44. Zhang D, et al. (2011) Drosophila katanin is a microtubule depolymerase that regulates cortical-microtubule plus-end interactions and cell migration. *Nat Cell Biol* 13:361–370.
45. Lindeboom JJ, et al. (2018) CLASP stabilization of plus ends created by severing promotes microtubule creation and reorientation. *J Cell Biol* 127:jcb.201805047.
46. Walker RA, Inoué S, Salmon ED (1989) Asymmetric behavior of severed microtubule ends after ultraviolet-microbeam irradiation of individual microtubules in vitro. *J Cell Biol* 108:931–937.
47. Tran PT, Walker RA, Salmon ED (1997) A metastable intermediate state of microtubule dynamic instability that differs significantly between plus and minus ends. *J Cell Biol* 138:105–117.
48. Howell B, Larsson N, Gullberg M, Cassimeris L (1999) Dissociation of the tubulin-sequestering and microtubule catastrophe-promoting activities of oncoprotein 18/stathmin. *Mol Biol Cell* 10:105–118.
49. Segerman B, Larsson N, Holmfeldt P, Gullberg M (2000) Mutational analysis of op18/stathmin-tubulin-interacting surfaces. Binding cooperativity controls tubulin GTP hydrolysis in the ternary complex. *J Biol Chem* 275:35759–35766.
50. Lohret TA, McNally FJ, Quarmby LM (1998) A role for katanin-mediated axonemal severing during Chlamydomonas deflagellation. *Mol Biol Cell* 9:1195–1207.
51. Yu W, et al. (2005) Regulation of microtubule severing by katanin subunits during neuronal development. *J Neurosci* 25:5573–5583.
52. Loughlin R, Wilbur JD, McNally FJ, Nédélec FJ, Heald R (2011) Katanin contributes to interspecies spindle length scaling in Xenopus. *Cell* 147:1397–1407.
53. Vale RD (1991) Severing of stable microtubules by a mitotically activated protein in Xenopus egg extracts. *Cell* 64:827–839.
54. Bowne-Anderson H, Hibbel A, Howard J (2015) Regulation of microtubule growth and catastrophe: Unifying theory and experiment. *Trends Cell Biol* 25:769–779.
55. Verde F, Dogterom M, Stelzer E, Karsenti E, Leibler S (1992) Control of microtubule dynamics and length by cyclin A- and cyclin B-dependent kinases in Xenopus egg extracts. *J Cell Biol* 118:1097–1108.
56. Komarova YA, Akhmanova AS, Kojima S, Galjart N, Borisy GG (2002) Cytoplasmic linker proteins promote microtubule rescue in vivo. *J Cell Biol* 159:589–599.
57. Al-Bassam J, et al. (2010) CLASP promotes microtubule rescue by recruiting tubulin dimers to the microtubule. *Dev Cell* 19:245–258.
58. Deinum EE, Tindemans SH, Lindeboom JJ, Mulder BM (2017) How selective severing by katanin promotes order in the plant cortical microtubule array. *Proc Natl Acad Sci USA* 114:6942–6947.
59. Yu W, et al. (2008) The microtubule-severing proteins spastin and katanin participate differently in the formation of axonal branches. *Mol Biol Cell* 19:1485–1498.
60. Lee H-H, Jan LY, Jan Y-N (2009) Drosophila IKK-related kinase Ik2 and Katanin p60-like 1 regulate dendrite pruning of sensory neuron during metamorphosis. *Proc Natl Acad Sci USA* 106:6363–6368.
61. Castoldi M, Popov AV (2003) Purification of brain tubulin through two cycles of polymerization-depolymerization in a high-molarity buffer. *Protein Expr Purif* 32:83–88.
62. Hyman A, et al. (1991) Preparation of modified tubulins. *Methods Enzymol* 196:478–485.
63. Gell C, et al. (2010) Microtubule dynamics reconstituted in vitro and imaged by single-molecule fluorescence microscopy. *Methods Cell Biol* 95:221–245.
64. Tseng Q, et al. (2011) A new micropatterning method of soft substrates reveals that different tumorigenic signals can promote or reduce cell contraction levels. *Lab Chip* 11:2231–2240.